

# Performance Tradeoff Between Overhead and Achievable SNR in RIS Beam Training

Friedemann Laue, *Graduate Student Member, IEEE*,

Vahid Jamali, *Member, IEEE*, and Robert Schober, *Fellow, IEEE*

## Abstract

Efficient beam training is the key challenge in the codebook-based configuration of reconfigurable intelligent surfaces (RISs) because the beam training overhead can have a strong impact on the achievable system performance. In this paper, we study the performance tradeoff between overhead and achievable signal-to-noise ratio (SNR) in RIS beam training while taking into account the size of the targeted coverage area, the RIS response time, and the delay for feedback transmissions. Thereby, we consider three common beam training strategies: full search (FS), hierarchical search (HS), and tracking-based search (TS). Our analysis shows that the codebook-based illumination of a given coverage area can be realized with wide- or narrow-beam designs, which result in two different scaling laws for the achievable SNR. Similarly, there are two regimes for the overhead, where the number of pilot symbols required for reliable beam training is dependent on and independent of the SNR, respectively. Based on these insights, we investigate the impact of the beam training overhead on the effective rate and provide an upper bound on the user velocity for which the overhead is negligible. Moreover, when the overhead is not negligible, we show that TS beam training achieves higher effective rates than HS and FS beam training, while HS beam training may or may not outperform FS beam training, depending on the RIS response time, feedback delay, and codebook size. Finally, we present numerical simulation results that verify our theoretical analysis. In particular, our results confirm the existence of the proposed regimes,

This work was presented in part at [1] (*Corresponding author: Friedemann Laue.*)

V. Jamali's work is supported in part by the German Research Foundation (DFG) under CRC MAKI and in part by the LOEWE initiative (Hesse, Germany) within the emergenCITY center.

F. Laue and R. Schober are with Institute for Digital Communications, Friedrich-Alexander-Universität Erlangen-Nürnberg (FAU), 91058 Erlangen, Germany (e-mail: friedemann.laue@fau.de, robert.schober@fau.de).

F. Laue is also with Fraunhofer IIS, Fraunhofer Institute for Integrated Circuits IIS, Division Communication Systems (e-mail: friedemann.laue@iis.fraunhofer.de).

V. Jamali is with Department of Electrical Engineering and Information Technology, Technical University of Darmstadt, 64283 Darmstadt, Germany (e-mail: vahid.jamali@tu-darmstadt.de).

reveal that fast RISs can lead to negligible overhead for FS beam training, and show that large feedback delays can significantly reduce the performance for HS beam training.

### Index Terms

Reconfigurable intelligent surface, codebook, beam training, mobility, overhead, tradeoff, SNR scaling law.

## I. INTRODUCTION

Reconfigurable intelligent surfaces (RISs) are a promising candidate technology for future wireless networks as they enable smartly configurable communication channels [2], [3]. RISs are nearly passive and low-cost devices comprising a large number of unit cells, each imposing an individual phase shift on an incident electromagnetic wave while reflecting it. By joint configuration of all unit-cell phase shifts, the characteristics of the RIS, e.g., the angle of reflection, can be controlled. Hence, tunable RISs create new opportunities for network design and are able to improve the system performance of next-generation wireless networks [4].

In order to maximize the system performance of RIS-assisted communication networks, the RIS phase shifts need to be optimized according to the instantaneous channel conditions. To this end, several frameworks for both phase-shift optimization and channel estimation have been proposed and recent surveys of such techniques can be found in [5], [6]. However, the complexity of the corresponding algorithms proposed in the literature typically scales with the number of RIS unit cells, which may lead to a prohibitively high computational burden for practical deployments [7]. In fact, it has been shown that thousands of RIS unit cells may be required to create a sufficiently strong reflected link for typical outdoor communication use cases [8], [9]. Therefore, low-complexity online algorithms for channel estimation and phase-shift optimization are key challenges for the deployment of large RISs.

### *A. Codebook-Based RIS Configuration*

One approach for reduction of the RIS configuration overhead is configuring the unit cells based on a predefined codebook, which is particularly suitable for line-of-sight (LoS)-dominated channels and high carrier frequencies [5]–[7], [10]. The advantage of codebook-based RIS configuration is twofold. First, the phase shifts for each codeword can be computed prior to deployment, which alleviates the potentially high complexity of online phase-shift design.

Second, explicit channel state information (CSI) is not required [7], [11]. Instead, the codeword providing the largest signal power at the receiver is selected via beam training. As a result, the overhead incurred by RIS configuration scales with the size of the codebook, which can be significantly smaller than the number of RIS unit cells [8], [12]. Moreover, for data transmission, the end-to-end channel resulting for a given codeword can be acquired adopting conventional channel estimation methods [7].

### *B. Performance Tradeoff of RIS Beam Training*

Generally speaking, RIS beam training can be considered as a form of implicit CSI acquisition, and there exists a fundamental tradeoff between the overhead afforded for CSI acquisition and the achievable signal-to-noise ratio (SNR) [7], [11], [13]–[15]. In other words, a larger amount of time spent for beam training results in a larger achievable SNR but, at the same time, reduces the time remaining for data transmission. For codebook-based RIS configuration, this tradeoff depends on the number of considered codewords, the phase-shift design of each codeword, the applied beam training strategy, and the velocity of the mobile users.

Moreover, there are additional restrictions that need to be considered for analyzing the performance tradeoff of RIS beam training. In particular, a communication system is usually subject to time constraints caused by hardware limitations and the employed communication protocol. For example, a RIS may be deployed in a standardized system like 3GPP new radio (NR), which prescribes a specific frame structure that inherently imposes a lower bound on the communication delay. Although low-latency applications have been targeted in recent NR releases, the user-plane and control-plane latencies are 1 ms and 10 ms, respectively; a reduction by a factor of ten is pursued for future releases [16], [17]. Nevertheless, this restriction on the communication delay can have an impact on the overhead of RIS beam training because beam training requires one or multiple transmissions of feedback information. Furthermore, hardware constraints can influence the achievable system performance because the adopted RIS technology and the RIS hardware design have an impact on the RIS response time, i.e., the time duration required for switching between two stable RIS configurations. Table I summarizes typical response times for current RIS technologies. For example, fast switching unit cells can be realized using PIN diodes, whereas liquid crystals increase the RIS response time by several orders of magnitude. However, liquid crystal technology is a promising solution for large-scale RISs because of the low manufacturing cost and low power consumption [18]. Thus, a comprehensive analysis of the performance of

TABLE I: Response Times for Current RIS Technologies [9].

Technology	Response Time	Comment
PIN diode	$\sim$ ns	Control circuits may reduce response times, 0.33 $\mu$ s to 28 $\mu$ s reported in [20]–[23].
MEMS	$\sim$ $\mu$ s	For example, 3 $\mu$ s to 20 ms reported in [24]–[26].
Liquid crystal	$\sim$ ms	10 ms measured for beam steering between $\pm 60^\circ$ [27].

RIS beam training should not only consider the properties of the adopted codebook and the employed beam training strategies, but also has to take into account hardware limitations and delay constraints [7], [19].

### C. Related Work and Contributions

Recently, beam training and codebook-based RIS configuration have been studied in several works [8], [11]–[15], [28]–[37]. Thereby, the main focus was on reducing the beam training overhead compared to a full search of the entire codebook. A popular approach is to employ hierarchically structured codebooks and multi-lobe beam patterns, which have been studied for both near field and far field deployments [11], [13], [30]–[32]. Moreover, the beam training overhead was reduced by exploiting deep-learning techniques [33], sensing at the RIS [34], two time scales of the RIS-assisted channel [35], and estimation of the angle of arrival (AoA) and angle of departure (AoD) based on random beamforming [36]. Similarly, prediction and tracking of the user position was investigated in [37].

However, only few existing works investigated the performance tradeoff between the beam training overhead and the achievable system performance [7], [11], [13]–[15]. For example, the authors of [13], [14] studied multi-lobe beam training for an intelligent omni-surface and showed that there exists an optimal codebook size maximizing the effective system throughput. Similar results were obtained for a reconfigurable refractive surface [15]. Furthermore, the relation between overhead and the success rate of beam training was studied in [11], where non-ideal beam patterns were taken into account.

Nevertheless, some important aspects have not been investigated, yet. For example, as shown

in Table I, the considered RIS technology has a strong impact on the RIS response time, which is an essential parameter of the beam training overhead and has to be taken into account for the tradeoff analysis. Similarly, the considered feedback delay can be relevant for the beam training overhead. Moreover, the RIS codebook is usually designed for covering the entire angular space, but, in practice, a typical deployment aims to illuminate a specific area only [7]. Thus, the codebook size can be reduced if the specifics of the target area are taken into account, which inherently reduces the beam training overhead. However, the relation between codebook size and coverage area has not been considered in the existing studies on RIS beam training. In addition, most existing works assume one pilot symbol per codeword during beam training, but, depending on the achievable RIS gain, additional pilot symbols may be required to select the optimal beam with high probability.

Motivated by the above discussion, this paper provides a comprehensive analysis of codebook-based RIS configuration and investigates the fundamental performance tradeoff between the beam training overhead and the achievable SNR. The main contributions of this paper can be summarized as follows:

- We show that codebook-based illumination of a target area by a RIS can be achieved with narrow- or wide-beam designs, which leads to two different fundamental regimes and scaling laws for the achievable SNR. In addition to the well-known quadratic scaling law for narrow-beam designs, we show that wide-beam designs result in a linear scaling of the SNR in both the RIS size and the codebook size.
- We show that there are also two regimes for the beam training overhead, characterized by the number of pilot symbols required for reliable beam training. In particular, our analysis reveals that the beam training overhead is either dependent on or independent of the SNR.
- We propose a general model for the overhead of multi-level beam training that accounts for the RIS response time, the feedback delay, and the velocity of a mobile user. Based on this model and the proposed regimes, we derive the overhead for reliable beam training for three common beam training strategies: full search (FS), hierarchical search (HS), and tracking-based search (TS).
- Assuming reliable beam training, we show that TS beam training achieves higher effective rates than FS and HS beam training, while we reveal that HS beam training may or may not outperform FS beam training, depending on the RIS response time, feedback delay, and codebook size. In addition, we provide upper bounds for the mobile user's velocity, which

guarantee that the beam training overhead has negligible impact on system performance.

- We present a comprehensive set of simulation results that corroborate our theoretical analysis. In particular, we verify the existence of the proposed regimes and validate the condition for negligible beam training overhead. Moreover, our simulation results reveal that fast RISs facilitate FS beam training, whereas large feedback delays can significantly reduce the performance for HS beam training.

The remainder of this paper is organized as follows. Section II describes the considered communication system. The different regimes for the SNR and the overhead are presented in Section III. A detailed analysis of the considered beam training strategies and the overheads they cause is provided in Section IV. These results are adopted in Section V to study the performance tradeoff of RIS beam training. Finally, numerical simulation results are presented in Section VI, and conclusions are drawn in Section VII.

*Notations:* Bold small and capital letters are used to denote vectors and matrices, respectively. The zero vector of size  $n$  and the identity matrix of size  $n \times n$  are represented by  $\mathbf{0}_n$  and  $\mathbf{I}_n$ , respectively. Moreover,  $(\cdot)^H$  denotes the Hermitian operator,  $\mathbb{E}[\cdot]$  represents expectation, and  $|\cdot|$  denotes the magnitude of a scalar or the cardinality of a set. The smallest integer larger than  $x$  is represented by  $\lceil x \rceil$ . Furthermore, a complex Gaussian distribution with mean vector  $\mathbf{m}$  and covariance matrix  $\mathbf{C}$  is denoted by  $\mathcal{CN}(\mathbf{m}, \mathbf{C})$ , and  $\mathcal{U}(a, b)$  denotes a uniform distribution in the interval  $[a, b]$ .

## II. SYSTEM MODEL

As illustrated in Fig. 1, we consider a narrow-band multiple-input single-output (MISO) communication system comprising a base station (BS), a RIS, and a mobile user that travels within a given coverage area of size  $A$ . Adopting a high carrier frequency, e.g., in the millimeter wave (mmWave) band, we assume LoS-dominated channels and a blocked direct link between the BS and the user [11]. Thus, the BS transmits data to the user via the RIS, where we assume that both the BS and the user are in the far-field of the RIS. The BS comprises  $N_{\text{BS}}$  antenna elements with element spacing  $d$  and antenna gain  $G_{\text{TX}}$ , and the user is equipped with a single antenna with gain  $G_{\text{RX}}$ . Moreover, we assume that the RIS and the coverage area are located in the  $x$ - $y$  and  $y$ - $z$  planes, respectively. At the RIS, the elevation and azimuth AoAs of the incident wave and AoDs of the reflected wave are denoted by  $(\theta_i, \phi_i)$  and  $(\theta_r, \phi_r)$ , respectively. Furthermore, we assume a square RIS comprising  $Q$  unit cells of lengths  $d_x$  and  $d_y$  along the

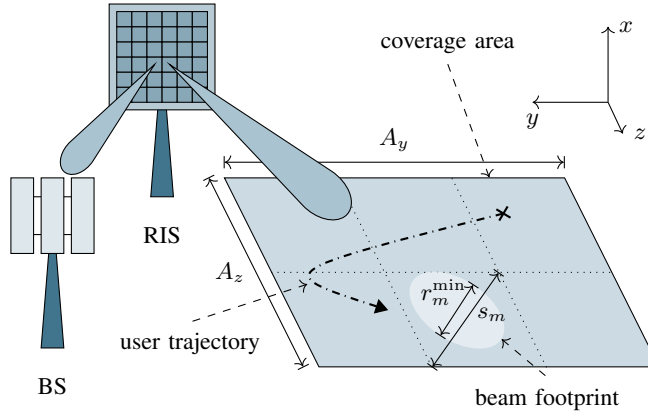


Fig. 1: RIS-assisted MISO system with a mobile user.

$x$ - and  $y$ -directions, respectively. In order to align the RIS reflection beam with the location of the mobile user, the RIS is regularly reconfigured by means of beam training. Thereby, in general, we assume a predefined multi-level RIS codebook with  $L$  levels<sup>1</sup>. The codewords at the  $l$ th level,  $l \in \{1, \dots, L\}$ , are designed to illuminate a particular subarea of the coverage area, respectively, and the set of codewords at the  $l$ th level is denoted by  $\mathcal{M}_l$ . In addition,  $\mathcal{M}_{t,l} \subseteq \mathcal{M}_l$  denotes the subset of codewords that are actually used for beam training, which is specified by the considered beam training strategy, see Section IV-A. Finally, the number of codewords in sets  $\mathcal{M}_l$  and  $\mathcal{M}_{t,l}$  are denoted by  $|\mathcal{M}_l| = M_l$  and  $|\mathcal{M}_{t,l}| = M_{t,l}$ , respectively.

#### A. Transmission and Beam Training Protocol

We consider a frame-based transmission protocol and assume that the frame duration  $T_f$  corresponds to the beam coherence time, i.e., the time duration for which the mobile user is covered by the beam of a given codeword. Thus, beam training is required once per frame. In this work, we assume downlink beam training, where the BS transmits pilot symbols to the user, while the RIS changes<sup>2</sup> its phase-shift configuration based on the predefined codebook.

As illustrated in Fig. 2, the first segment of a frame is determined by the total beam training overhead  $\tau_t$  resulting from beam training with  $L$  codebook levels. In particular, at the  $l$ th level,

<sup>1</sup>In Section IV, we study FS beam training and TS beam training with  $L = 1$  as well as HS beam training with  $L > 1$ .

<sup>2</sup>In practice, beam training requires synchronization between user, BS, and RIS, which may increase the overall overhead. However, we neglect the impact of synchronization in this work because synchronization errors below 500 ns can be realized with recent releases of 3GPP NR [16], [38], which is smaller than the symbol duration of the considered narrow-band system.

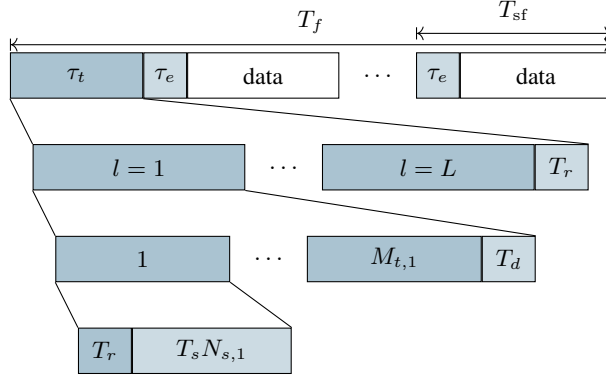


Fig. 2: Illustration of one frame of the considered transmission protocol.

each codeword in  $\mathcal{M}_{t,l}$  causes an overhead of  $T_r + T_s N_{s,l}$ , where  $T_r$ ,  $T_s$ , and  $N_{s,l}$  denote the RIS response time (i.e., the time needed by the RIS to change from one phase-shift configuration to another, see Table I), the pilot symbol duration, and the number of pilot symbols, respectively. In addition, at each codebook level, the user determines the codeword that provides the largest received signal power and transmits the corresponding codeword index  $m_l^*$  over a dedicated feedback channel to the RIS, which introduces a delay of  $T_d$ . Then, assuming zero processing delay<sup>3</sup>,  $m_l^*$  is used to determine the subset of codewords for the training at level  $l + 1$ . Finally, beam training is concluded by configuring codeword  $m_l^*$  for subsequent data transmission, which adds a further overhead of  $T_r$ . Thus, the total beam training overhead is given by

$$\tau_t = T_r + LT_d + \sum_{l=1}^L (T_r + T_s N_{s,l}) M_{t,l}. \quad (1)$$

After beam training, the RIS configuration is fixed to estimate the end-to-end channel for data transmission. To this end, we adopt the channel coherence time in [39, Eq. (4.40.c)] to divide the remaining time  $T_f - \tau_t$  into subframes of duration  $T_{sf} = \sqrt{\frac{9}{16\pi}} \frac{\lambda}{v}$ , where  $\lambda$  and  $v$  denote the wavelength and the mobile user's velocity, respectively. Thus, assuming a channel estimation overhead of  $\tau_e$  in each subframe, the overall overhead for beam training and channel estimation normalized by the frame duration is given by

$$\bar{\tau} = \frac{\tau_t + \frac{T_f - \tau_t}{T_{sf}} \tau_e}{T_f} = \frac{\tau_t}{T_f} (1 - \bar{\tau}_e) + \bar{\tau}_e, \quad (2)$$

<sup>3</sup>We only focus on the systematic overhead of the considered beam training protocol and neglect possible processing overheads. In practice,  $\mathcal{M}_{l+1}$  may be found based on  $m_l^*$  using a simple look-up table.

where  $\bar{\tau}_e = \tau_e/T_{\text{sf}} = \tau_e 4\sqrt{\pi}v/(3\lambda)$  denotes the normalized estimation overhead, and we assume that  $\frac{T_f - \tau_t}{T_{\text{sf}}}$  is an integer.

### B. Signal Model

During beam training, the received signal for the  $m$ th codeword is given by

$$\mathbf{y}_m = \sqrt{G_{\text{RX}}G_{\text{TX}}P}\mathbf{h}_m^H\mathbf{f}\mathbf{x} + \mathbf{n}, \quad (3)$$

where  $\mathbf{x} \in \mathbb{C}^{N_{s,l}}$ ,  $\mathbf{h}_m \in \mathbb{C}^{N_{\text{BS}}}$ ,  $\mathbf{f} \in \mathbb{C}^{N_{\text{BS}}}$ ,  $P$ , and  $\mathbf{n} \sim \mathcal{CN}(\mathbf{0}_{N_{s,l}}, \sigma^2\mathbf{I}_{N_{s,l}})$  denote the transmit vector comprising  $N_{s,l}$  pilot symbols of unit power, the end-to-end BS-RIS-user channel for the  $m$ th codeword, the precoding vector at the BS, the transmit power, and zero-mean Gaussian noise with power  $\sigma^2$ , respectively. The precoding vector  $\mathbf{f}$  is chosen to align the main lobe of the BS with the LoS path to the RIS [11], and the end-to-end channel  $\mathbf{h}_m$  is given by<sup>4</sup>

$$\mathbf{h}_m^H = \mathbf{h}_r^H \mathbf{G}_m \mathbf{H}_i, \quad (4)$$

where  $\mathbf{H}_i \in \mathbb{C}^{Q \times N_{\text{BS}}}$ ,  $\mathbf{G}_m \in \mathbb{C}^{Q \times Q}$ , and  $\mathbf{h}_r \in \mathbb{C}^Q$  denote the BS-RIS channel matrix, the reflection matrix of the RIS, and the RIS-user channel vector, respectively. For  $\mathbf{H}_i$  and  $\mathbf{h}_r$ , we assume a statistical channel model<sup>5</sup> with a dominant LoS path. Moreover, the RIS reflection matrix is given by  $\mathbf{G}_m = \text{diag}\left(\left[g_{\text{UC}}e^{j\psi_{m,1}} \quad g_{\text{UC}}e^{j\psi_{m,2}} \quad \dots \quad g_{\text{UC}}e^{j\psi_{m,Q}}\right]\right)$ , where  $g_{\text{UC}}$  and  $\psi_{m,q}$  denote the unit-cell factor and the phase shift of the  $q$ th unit cell, respectively. The unit cell factor is given by  $g_{\text{UC}} = \frac{j4\pi d_x d_y}{\lambda^2} \tilde{g}_{\text{UC}}$ , where  $\tilde{g}_{\text{UC}}$  accounts for the RIS AoAs and AoDs and the polarization of the incident wave, see [8] for details.

### C. System Performance Metrics

For data transmission, it is desired that the selected codeword maximizes the end-to-end channel gain  $|\sqrt{G_{\text{RX}}G_{\text{TX}}P}\mathbf{h}_m^H\mathbf{f}|^2$  in (3), which is achieved by matched-filtering the received training signal with the known pilot sequence. Hence, the codeword selection at the  $l$ th codebook level is given by

$$m_l^* = \arg \max_{m \in \mathcal{M}_{t,l}} |\mathbf{x}^H \mathbf{y}_m|^2. \quad (5)$$

<sup>4</sup>Since the direct BS-user link is assumed to be blocked, its contribution to  $\mathbf{h}_m$  is neglected. Thus, (4) only comprises the BS-RIS-user link.

<sup>5</sup>For example, we adopt a geometric Rician fading channel model for our numerical simulations, see Section VI.

Based on the filtered training signal, we define the training SNR as follows

$$\gamma_{m,l} = \frac{G_{\text{RX}}G_{\text{TX}}PN_{s,l}|\mathbf{h}_m^H \mathbf{f}|^2}{\sigma^2} = N_{s,l}\bar{\gamma}_{m,l}, \quad (6)$$

where  $\bar{\gamma}_{m,l} = G_{\text{RX}}G_{\text{TX}}P|\mathbf{h}_m^H \mathbf{f}|^2/\sigma^2$  denotes the achievable SNR per symbol for the  $m$ th codeword at the  $l$ th codebook level.

Moreover, we aim to analyze the system performance by evaluating the tradeoff between the achievable SNR for data transmission and the overall beam training overhead. The latter is given by  $\bar{\tau}$  in (2). The former, assuming a unit-power data symbol, is given by

$$\gamma^* = \bar{\gamma}_{m_L^*,L} = \frac{G_{\text{RX}}G_{\text{TX}}P|\mathbf{h}_{m_L^*}^H \mathbf{f}|^2}{\sigma^2}. \quad (7)$$

Thus, the performance tradeoff can be analyzed based on the effective ergodic rate

$$R = (1 - \bar{\tau}) \mathbb{E}[\log_2(1 + \gamma^*)]. \quad (8)$$

In the following sections, we analyze  $\gamma^*$  and  $\bar{\tau}$  in detail to reveal their impact on (8).

*Remark 1.* The probability of selecting the best codeword during beam training depends on several parameters. For example, receiver noise and channel fading have an impact on the instantaneous signal power  $|\mathbf{x}^H \mathbf{y}_m|^2$  in (5), which may lead to a suboptimal codeword selection. Similarly, beam training is influenced by the codebook design because it affects the beam patterns and thus the received power for a particular codeword [11]. Moreover, erroneous codeword selection in multi-level beam training propagates from one level to the next, which may result in beam misalignment [19]. Since reliable beam training is desired, we propose two regimes for the beam training overhead in Section III-B, which guarantee that the training SNR in (6) is sufficiently large to ensure selection of the best beam possible. Nevertheless, the effect of erroneous codeword selection is included in our numerical results in Section VI.

### III. REGIMES FOR SNR AND OVERHEAD

This section introduces fundamental regimes for both the achievable SNR and the beam training overhead, which form the basis for the beam training analysis in Section IV and the tradeoff analysis in Section V.

### A. Achievable SNR

The achievable SNR for codebook-based RIS configuration can be characterized by two fundamental regimes, which depend, among other parameters, on the size of the considered codebook [1]. In the following, we provide a general definition of these SNR regimes, which takes the beam width and the size of the coverage area into account<sup>6</sup>. To this end, without loss of generality, we first focus on the  $m$ th codeword and the  $m$ th subarea for the  $l$ th codebook level, and introduce the following definitions of narrow beams and wide beams. For a narrow beam, the phase shifts for the  $m$ th codeword are designed to maximize the received power for particular values of  $(\theta_r, \phi_r)$ , e.g., for the AoDs from the RIS to the center of the  $m$ th subarea. Such a design yields the minimum possible beam width and results in the smallest diameter of the beam footprint, denoted by  $r_m^{\min}$ , see Fig. 1. For a wide beam, in contrast, the phase shifts are designed for non-degenerate intervals of  $(\theta_r, \phi_r)$ , which leads to beam footprints wider than  $r_m^{\min}$ .

*Proposition 1.* If the  $m$ th codeword at the  $l$ th codebook level is designed to fully illuminate the  $m$ th subarea, the achievable SNR  $\bar{\gamma}_{m,l}$  scales as follows

$$\bar{\gamma}_{m,l} \propto \begin{cases} QM_l & r_m^{\min} \ll s_m \\ Q^2 & r_m^{\min} \gg s_m, \end{cases} \quad (9)$$

where  $s_m$  denotes the diameter of the  $m$ th subarea.

*Proof.* If  $r_m^{\min} \ll s_m$  holds, the footprint of a narrow beam is not wide enough to fully illuminate the targeted subarea, i.e., a wide-beam design is required to obtain the desired coverage. In this work, we adopt an idealized wide-beam design that perfectly reflects the power collected at the RIS to the targeted subarea, because the RIS gain for existing wide-beam designs is usually not in tractable analytical form [28], [40]. For the idealized wide-beam design, it is shown in Appendix A1 that  $\bar{\gamma}_{m,l} \propto QM_l$ . In contrast, if  $r_m^{\min} \gg s_m$  holds, a narrow beam is sufficient to fully illuminate the targeted subarea, which results in  $\bar{\gamma}_{m,l} \propto Q^2$ , see Appendix A2.  $\square$

Based on Proposition 1, we define the following regimes for the achievable SNR for codebook-based RIS configuration. The system operates in the wide-beam regime (WBR) if  $r_m^{\min} \ll s_m$  holds for all codewords  $m \in \mathcal{M}_l$  at the  $l$ th codebook level. Then, wide beams are required to fully illuminate the subareas of the coverage area and  $\bar{\gamma}_{m,l} \propto QM_l$ . In contrast, the system

<sup>6</sup>We only focus on the reflected beam from the RIS to the user because the incident beam is aligned with the LoS path to the BS.

operates in the narrow-beam regime (NBR) if  $r_m^{\min} \gg s_m$  holds for all codewords  $m \in \mathcal{M}_l$  at the  $l$ th codebook level. In this case, narrow beams are sufficient to fully illuminate the subareas of the coverage area and  $\bar{\gamma}_{m,l} \propto Q^2$ . We note that the transition between the WBR and the NBR is gradual and continuous. Although this transition regime is not captured in Proposition 1, the SNRs in the WBR and the NBR can be considered as lower and upper bounds for the transition regime, respectively. Therefore, this paper focuses on the WBR and NBR, and leaves a detailed analysis of the transition regime for future work.

In order to obtain more insight on the SNR regimes, consider the following assumptions on the coverage area and the codebook. We assume a rectangular coverage area with center coordinates  $(x_A, y_A, z_A)$  and size  $A = A_y A_z$ , where  $A_y$  and  $A_z$  denote the side lengths in the  $y$ - and  $z$ -directions, respectively. The coverage area is illuminated by  $M_l = M_{l,x} M_{l,y}$  codewords, i.e., the codebook at the  $l$ th level comprises  $M_{l,x}$  and  $M_{l,y}$  different phase-shift profiles along the  $x$ - and  $y$ -directions of the RIS, respectively, indexed by  $m_x \in \{1, \dots, M_{l,x}\}$  and  $m_y \in \{1, \dots, M_{l,y}\}$ . This corresponds to partitioning the coverage area into  $M_l$  subareas, each of size  $(A_y/M_{l,y})(A_z/M_{l,x})$ . Furthermore, assume that the beam of the  $m$ th codeword is directed to the center of the  $(m_x, m_y)$ th subarea, which is located at distance  $d_m^2 = x_A^2 + \left(y_A + \frac{A_y}{2M_{l,y}}(2m_y - 1 - M_{l,y})\right)^2 + \left(z_A + \frac{A_z}{2M_{l,x}}(2m_x - 1 - M_{l,x})\right)^2$  from the RIS. Then, the minimum diameter of the beam footprint is given by  $r_m^{\min} = 2d_m \tan(\Delta\theta^{\min}/2)$ , where  $\Delta\theta^{\min}$  denotes the minimum angular beam width of a narrow beam. The latter, assuming half-wavelength sized unit cells and the 3 dB beam width in broadside direction, is given by  $\Delta\theta^{\min} = \left|\frac{\pi}{2} - \arccos\left(\frac{2.782}{\pi\sqrt{Q}}\right)\right| + \left|\frac{\pi}{2} - \arccos\left(\frac{-2.782}{\pi\sqrt{Q}}\right)\right|$  [41, Eq. (27)]. Consequently, we obtain

$$r_m^{\min} = 2d_m \tan(\Delta\theta^{\min}/2) \approx 1.77 \frac{d_m}{\sqrt{Q}}, \quad (10)$$

where the approximation is based on  $\tan(x) \approx x$  and  $\arccos(x) \approx \frac{\pi}{2} - x$  for  $|x| < 0.5$ , which can be assumed since usually  $Q > 13 > 16(2.782/\pi)^2$ . As a result, the WBR and NBR can be characterized by  $Q$ ,  $A$ , and  $M_l$  as follows.

*Lemma 1.* The system operates in the WBR if

$$Q \gg \frac{(1.77 \max_{m \in \mathcal{M}_l} d_m)^2}{(A_y/M_{l,y})^2 + (A_z/M_{l,x})^2}. \quad (11)$$

On the contrary, the system operates in the NBR if

$$Q \ll \frac{(1.77 \min_{m \in \mathcal{M}_l} d_m)^2}{(A_y/M_{l,y})^2 + (A_z/M_{l,x})^2}. \quad (12)$$

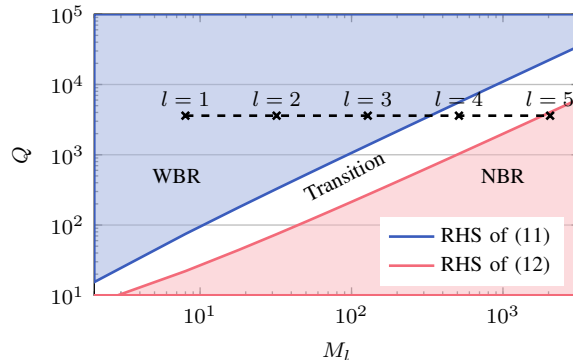


Fig. 3: SNR regimes WBR and NBR as functions of  $M_l$  and  $Q$ , visualized based on the right-hand sides of (11) and (12) for  $(x_A, y_A, z_A) = (-10 \text{ m}, -20 \text{ m}, 100 \text{ m})$ , and  $A = 100 \text{ m} \times 50 \text{ m}$ .

*Proof.* Since all subareas have equal size, we have

$$s_m = \sqrt{(A_y/M_{l,y})^2 + (A_z/M_{l,x})^2} \quad (13)$$

for all codewords. Thus, according to the above definition of the SNR regimes, the system operates in the WBR and NBR for  $\max_{m \in \mathcal{M}_l} r_m^{\min} \ll s_m$  and  $\min_{m \in \mathcal{M}_l} r_m^{\min} \gg s_m$ , respectively, which can be rewritten as (11) and (12) using (10) and (13).  $\square$

The results of Lemma 1 are visualized in Fig. 3, which shows the impact of the codebook size and the RIS size on the SNR regimes. For visualization purpose, we adopt the right-hand sides (RHSs) of (11) and (12) to separate the WBR and NBR, although there is a continuous transition in practice. Nevertheless, Fig. 3 suggests that the WBR is particularly relevant for very large RISs or small codebooks, e.g., at the lower levels of a hierarchical codebook. Moreover, for  $L > 1$ , the SNR regime may change during beam training, which is indicated by the markers in Fig. 3 assuming  $Q = 3600$  and  $L = 5$ . In particular, one can see that for the beam training in levels  $l \leq 3$  the WBR is relevant, whereas for  $l = 4$  and  $l = 5$  the transition regime and the NBR apply, respectively. This observation is confirmed by our numerical results in Section VI-B, where Fig. 5 shows that the SNR changes from linear scaling (WBR) to saturation (NBR) as the codebook size grows.

### B. Beam Training Overhead

Next, we show that the beam training overhead is also characterized by two fundamental regimes, in which  $\tau_t$  is dependent on and independent of the SNR, respectively. To this end, recall that the

beam training is influenced by receiver noise and channel fading, which may affect the codeword selection in (5). Thus, in order to ensure that the selected codeword is correctly aligned with the current user location with high probability, we require that the optimal codeword at each level achieves a minimum SNR at the user. As a result, we assume that reliable beam training is possible if  $\max_{m \in \mathcal{M}_{t,l}} \gamma_{m,l} \geq \gamma_{\min}$ , which by using (6) can be rewritten as

$$N_{s,l} \geq \frac{\gamma_{\min}}{\bar{\gamma}_l}, \quad (14)$$

where  $\bar{\gamma}_l = \max_{m \in \mathcal{M}_{t,l}} \bar{\gamma}_{m,l}$ . Based on (14), we define two overhead regimes as follows. If  $N_{s,l} \geq \gamma_{\min}/\bar{\gamma}_l > 1$ , more than one pilot symbol is required for reliable beam training, which we refer to as the multiple pilot symbol regime (MPR). In this case, the beam training overhead in (1) is a function of the SNR. Moreover, we set  $N_{s,l} = 1$  if  $\gamma_{\min}/\bar{\gamma}_l < 1$  because at least one pilot symbol is always required. In this case, the beam training overhead in (1) is independent of the SNR, and we refer to this regime as the single pilot symbol regime (SPR).

Furthermore, it is worth noting that the MPR overhead regime is linked with the WBR and the NBR because  $\bar{\gamma}_l$  follows the scaling laws in (9). In order to include these regimes in (14), we adopt (37) and (40) in Appendix A to rewrite  $\bar{\gamma}_l = \tilde{\gamma}^{\text{WBR}} Q M_l$  and  $\bar{\gamma}_l = \tilde{\gamma}^{\text{NBR}} Q^2$  for the WBR and the NBR, respectively, where  $\tilde{\gamma}^{\text{WBR}} = \frac{P G_{\text{TX}} N_{\text{BS}} G_{\text{RX}} \lambda^2 d_x d_y \bar{a}_{\text{RIS}}}{\sigma^2 (4\pi d_i)^2 A}$  and  $\tilde{\gamma}^{\text{NBR}} = \frac{P G_{\text{TX}} N_{\text{BS}} G_{\text{RX}} \lambda^2 \lambda^2 |g_{\text{UC}}|^2}{\sigma^2 (4\pi d_i)^2 (4\pi d_r)^2}$ . Note that the max operator has been dropped because (37) and (40) hold for the codeword that optimally illuminates the user location, i.e., the codeword that maximizes  $\bar{\gamma}_{m,l}$ . As a result, (14) can be rewritten as

$$N_{s,l} \geq \begin{cases} \frac{\gamma_{\min}}{\tilde{\gamma}^{\text{WBR}} Q M_l} & \text{WBR} \\ \frac{\gamma_{\min}}{\tilde{\gamma}^{\text{NBR}} Q^2} & \text{NBR.} \end{cases} \quad (15)$$

*Remark 2.* One can see from (1) that the beam training overhead can be reduced by reducing the pilot symbol duration  $T_s$ . However, this is only possible for high SNRs, where  $N_{s,l} \gg \gamma_{\min}/\bar{\gamma}_l$  holds, as can be seen from the following example. Assume that one pilot symbol is just sufficient for reliable beam training, i.e., we have  $\gamma_{\min}/\bar{\gamma}_l = 1$ . In this case, we can use  $N_{s,l} = 1$ . On the other hand,  $\bar{\gamma}_l \propto 1/\sigma^2 \propto T_s$  because the noise power  $\sigma^2$  scales with the signal bandwidth and is thus inversely proportional to the symbol duration. Consequently, decreasing  $T_s$  leads to  $\gamma_{\min}/\bar{\gamma}_l > 1$  and  $N_{s,l} > 1$  is required to satisfy (14). In other words, the positive effect of a shorter pilot symbol duration on the beam training overhead is compensated by the additional pilot symbols required.

#### IV. BEAM TRAINING ANALYSIS

This section describes the considered FS, HS, and TS beam training strategies, and provides detailed analysis of their respective overheads. More specifically, we derive  $\tau_t$  in (1) and  $\bar{\tau}$  in (2) considering the different regimes for both overhead and achievable SNR. In the following, we refer to a particular beam training strategy using superscript  $x \in \{\text{FS}, \text{HS}, \text{TS}\}$ .

##### A. Beam Training Strategies

For each beam training strategy, we first define the corresponding codeword sets  $\mathcal{M}_l$  and  $\mathcal{M}_{t,l}$ . Then, using (1) and (15), we derive the overhead that is required for reliable beam training.

1) *Full Search*: FS beam training is the most robust scheme that selects the optimal codeword according to (5) because the entire codebook is searched and there is no dependence on previous decisions. Hence, we have  $L = 1$  and  $\mathcal{M}_l = \mathcal{M}_{t,l}$ , which implies  $M_{t,l} = M_l = M_L$ . Then, the beam training overhead is given by

$$\tau_t^{\text{FS}} \geq T_r (1 + M_L) + T_d + T_s \tilde{\tau}^{\text{FS}}, \quad (16)$$

where<sup>7</sup>

$$\tilde{\tau}^{\text{FS}} = \begin{cases} M_L & \text{SPR,} \\ \frac{1}{\tilde{\gamma}^{\text{WBR}}} \frac{\gamma_{\min}}{Q} & \text{MPR, WBR,} \\ \frac{M_L}{\tilde{\gamma}^{\text{NBR}Q}} \frac{\gamma_{\min}}{Q} & \text{MPR, NBR.} \end{cases} \quad (17)$$

2) *Hierarchical Search*: HS beam training is a commonly adopted method that requires less overhead than FS beam training [11], [30], [42]. In this work, we adopt a hierarchically structured codebook with  $L > 1$  levels and assume the following scheme. Beam training starts with a full search over all codewords at level  $l = 1$ , i.e.,  $\mathcal{M}_1 = \mathcal{M}_{t,1}$  and  $M_1 = M_{t,1}$ . At each subsequent level, the training set  $\mathcal{M}_{t,l}$  is determined by the subarea illuminated by codeword  $m_{l-1}^*$ , which is further divided into  $\tilde{M} = |\mathcal{M}_{t,l}|$  parts. Since  $\tilde{M}$  is usually small, we note that  $M_1 > \tilde{M}$  may be required to achieve a sufficiently large SNR at the first codebook level. Hence, the codebook

<sup>7</sup>Since the overhead only depends on the SNR if the system operates in the MPR, we consider three cases: (1) SPR, (2) MPR and WBR, and (3) MPR and NBR. Moreover, the overheads in the WBR and the NBR constitute upper and lower bounds for the transition regime, respectively, cf. Section III-A.

size at the  $l$ th level is given by  $|\mathcal{M}_l| = M_l = M_1 \tilde{M}^{l-1}$ , but only  $\zeta = M_1 + (L-1)\tilde{M}$  codewords are used for beam training. Consequently, the beam training overhead is given by

$$\tau_t^{\text{HS}} \geq T_r (1 + \zeta) + T_d L + T_s \sum_{l=1}^L \tilde{\tau}_l^{\text{HS}}, \quad (18)$$

where

$$\tilde{\tau}_l^{\text{HS}} = \begin{cases} M_{t,l} & \text{SPR,} \\ \frac{M_{t,l}}{\tilde{\gamma}^{\text{WBR}} M_l} \frac{\gamma_{\min}}{Q} & \text{MPR, WBR,} \\ \frac{M_{t,l}}{\tilde{\gamma}^{\text{NBR}} Q} \frac{\gamma_{\min}}{Q} & \text{MPR, NBR.} \end{cases} \quad (19)$$

3) *Tracking-Based Search*: In order include a beam training strategy with very low overhead in our analysis, we adopt a tracking-based scheme that exploits prior information, e.g., an approximate user location. Similar to FS beam training, TS beam training uses a single-level codebook, i.e.,  $L = 1$  and  $M_l = M_L$ . However, TS beam training exploits knowledge of the codeword that has been selected in the previous frame, in particular,  $\mathcal{M}_{t,l}$  is determined by the local environment of the previously illuminated subarea [1]. Assuming that the subareas are arranged in a regular grid, the local environment is defined by  $M_{t,l} = 8$  codewords. Ideally, scanning the local environment is sufficient to continuously track the mobile user without reinitialization<sup>8</sup>. Thus, the beam training overhead is given by

$$\tau_t^{\text{TS}} \geq T_r (1 + 8) + T_d + T_s \tilde{\tau}^{\text{TS}}, \quad (20)$$

where

$$\tilde{\tau}^{\text{TS}} = \begin{cases} 8 & \text{SPR,} \\ \frac{8}{\tilde{\gamma}^{\text{WBR}} M_L} \frac{\gamma_{\min}}{Q} & \text{MPR, WBR,} \\ \frac{8}{\tilde{\gamma}^{\text{NBR}} Q} \frac{\gamma_{\min}}{Q} & \text{MPR, NBR.} \end{cases} \quad (21)$$

### B. Overall Overhead

Next, we use the results in (16), (18), and (20) to define the overall overhead  $\bar{\tau}$  for FS, HS, and TS beam training. In contrast to beam training overhead  $\tau_t$ , overall overhead  $\bar{\tau}$  includes the

<sup>8</sup>Reinitialization and initial beam training in general require beam training strategies such as FS or HS, which cause additional overhead.

frame duration and the channel estimation overhead, which are relevant for the effective rate in (8).

Recall that frame duration  $T_f$  corresponds to the duration for which the mobile user is assumed to stay within one subarea, which is mainly determined by user velocity  $v$ , the user trajectory, and the sizes of the subareas. Since the user trajectory is usually unknown [15], we propose a parameterized model for the frame duration as follows. As a reference, let  $s_{\min} = \min_{m \in \mathcal{M}_L} s_m$  denote the shortest diagonal path through a subarea. Then, we assume that the user travels a distance of  $p = \nu s_{\min}$  through a subarea, where frame factor  $\nu > 0$  is a design parameter<sup>9</sup> to account for arbitrary user trajectories. Moreover, we note that  $s_{\min} \propto 1/M_L$  if a given coverage area is fully illuminated by  $M_L$  beams. Thus, we define  $s_{\min} = \mu/M_L$ , where  $\mu$  is specified by the considered sizes and shapes of the subareas. For example, as assumed for Lemma 1, if the coverage area is partitioned into rectangular subareas of equal size,  $s_{\min} = \sqrt{(A_y/M_{L,y})^2 + (A_z/M_{L,x})^2}$  and  $\mu = \sqrt{(A_y M_{L,x})^2 + (A_z M_{L,y})^2}$ , cf. (13). Based on these assumptions, the frame duration is parameterized as follows

$$T_f = \frac{p}{v} = \frac{\nu}{v} \frac{\mu}{M_L}. \quad (22)$$

Substituting (22) in (2) results in  $\bar{\tau} = \tau_t \frac{\nu M_L}{\nu \mu} (1 - \bar{\tau}_e) + \bar{\tau}_e$ , which is rewritten for notational simplicity as

$$\bar{\tau} = \alpha M_L \tau_t + \bar{\tau}_e, \quad (23)$$

where  $\alpha = \frac{\nu}{\nu \mu} (1 - \bar{\tau}_e)$ . Substituting (16), (18), and (20) in (23) results in the following overall overheads for reliable beam training

$$\bar{\tau}^{\text{FS}} \geq \alpha M_L [T_r (1 + M_L) + T_d + T_s \tilde{\tau}^{\text{FS}}] + \bar{\tau}_e, \quad (24)$$

$$\bar{\tau}^{\text{HS}} \geq \alpha M_L \left[ T_r (1 + \zeta) + T_d L + T_s \sum_{l=1}^L \tilde{\tau}_l^{\text{HS}} \right] + \bar{\tau}_e, \quad (25)$$

$$\bar{\tau}^{\text{TS}} \geq \alpha M_L [T_r (1 + 8) + T_d + T_s \tilde{\tau}^{\text{TS}}] + \bar{\tau}_e. \quad (26)$$

## V. PERFORMANCE TRADEOFF

In this section, we study the performance tradeoff between the overall overhead and the achievable SNR for RIS beam training. First, we analyze the relevance of the overhead and provide

<sup>9</sup>Although the user's path through a subarea may be larger than  $s_{\min}$ ,  $\nu < 1$  results in a good balance between beam training overhead and correct beam alignment. A similar approach was adopted in [43], where  $\nu$  was used to reduce the beam coherence time in order to capture impairments in practical systems.

an upper bound on  $v$ , which guarantees that codebook-based RIS configuration has a negligible impact on the system performance. Then, we show how FS, HS, and TS beam training lead to different effective rates if the overhead is not negligible.

### A. Relevance of Overhead

From (8), one can see that a performance tradeoff between overhead and achievable SNR only exists if the overall overhead  $\bar{\tau}$  is sufficiently large. Moreover, we note that the overall overhead is strongly influenced by the mobile user's velocity because it affects both the subframe duration and the frame duration. This fundamental relation between  $\bar{\tau}$  and  $v$  is described by the following proposition.

*Proposition 2.* The overall overhead is a quadratic function of the user velocity and has the form  $\bar{\tau} = (a + b)v - abv^2$ , where  $a = \frac{M_L \tau_t}{\nu \mu}$  and  $b = \frac{\tau_e^4 \sqrt{\pi}}{3\lambda}$ .  $\bar{\tau}$  is a concave parabola and the maximum value is greater or equal to one.

*Proof.* By definition of  $\alpha$  and  $\bar{\tau}_e$ , (23) can be written as  $\bar{\tau} = \frac{v}{\nu \mu} \left(1 - \frac{\tau_e^4 \sqrt{\pi} v}{3\lambda}\right) M_L \tau_t + \frac{\tau_e^4 \sqrt{\pi} v}{3\lambda} = (a + b)v - abv^2$  for  $a = \frac{M_L \tau_t}{\nu \mu}$  and  $b = \frac{\tau_e^4 \sqrt{\pi}}{3\lambda}$ . Since  $ab > 0$ ,  $\bar{\tau}$  is a concave parabola (opening to the bottom). Thus, the maximum value is given by the vertex of the parabola, which is found by evaluating  $\frac{d}{dv} \bar{\tau} = 0$  and given by  $\max_v \bar{\tau} = \frac{(a+b)^2}{4ab}$  at  $v = \frac{a+b}{2ab}$ . Since  $ab > 0$ , one can rewrite  $\frac{(a+b)^2}{4ab} \geq 1$  as  $(a - b)^2 \geq 0$ , which always holds. Therefore,  $\max_v \bar{\tau} \geq 1$ .  $\square$

We note that, although  $\bar{\tau}$  is a quadratic function of the user velocity, the overall overhead does not quadratically grow with  $v$ . Instead, since  $\frac{d}{dv} \bar{\tau} = a + b - 2abv$ , the gradient of  $\bar{\tau}$  is a linearly decreasing function with a maximum value of  $a + b$  at  $v = 0$ .

Furthermore, we note that the impact of  $\bar{\tau}$  on the effective rate in (8) is negligible if  $\bar{\tau} < \epsilon$ ,  $0 \leq \epsilon \ll 1$ . Based on Proposition 2, this condition for the overall overhead leads to an upper bound for the mobile user's velocity.

*Lemma 2.* The overall overhead has negligible impact, i.e.,  $\bar{\tau} < \epsilon$ , on the effective rate if  $v < \frac{a+b - \sqrt{(a+b)^2 - 4ab\epsilon}}{2ab}$ .

*Proof.* Since  $\bar{\tau}$  is a quadratic function in  $v$ , solving  $\bar{\tau} < \epsilon$  for  $v$  leads to the lower bound  $v > \frac{a+b + \sqrt{(a+b)^2 - 4ab\epsilon}}{2ab}$  and the upper bound  $v < \frac{a+b - \sqrt{(a+b)^2 - 4ab\epsilon}}{2ab}$ , which are always distinct because  $(a + b)^2 - 4ab\epsilon > 0$  due to  $\epsilon < 1$  and  $\frac{(a+b)^2}{4ab} \geq 1$ . However, only the upper bound for  $v$  is a feasible solution because the lower bound leads to zero time for data transmission, see Appendix B.  $\square$

Lemma 2 can be applied to FS, HS, or TS beam training, each resulting in a different upper bound on  $v$ . In order to remove this dependence on a particular beam training strategy, one can find a generalized bound on  $v$  as follows.

*Corollary 1.* Regardless of whether FS, HS, or TS beam training is employed, the overhead for codebook-based RIS configuration has negligible impact on the effective rate if

$$v < v^{\max} = \frac{a' + b - \sqrt{(a' + b)^2 - 4a'b\epsilon}}{2a'b}, \quad (27)$$

where  $a' = \frac{M_L \tau_t^{\max}}{\nu \mu}$  and  $\tau_t^{\max} = 1.25 N_{s,L} M_L T_s + (1 + M_L) T_r + L T_d$ .

*Proof.* Based on (23), one can see that  $\bar{\tau}$  increases with  $\tau_t$  because  $\alpha > 0$ . Thus, the overall overhead is bounded as  $\bar{\tau} \leq \bar{\tau}' = \alpha M_L \tau_t^{\max} + \bar{\tau}_e$ , where  $\tau_t^{\max} \geq \max_{x \in \{\text{FS, HS, TS}\}} \tau_t^x$  denotes an upper bound for the beam training overhead. For the problem at hand, we find  $\tau_t^{\max} = 1.25 N_{s,L} M_L T_s + (1 + M_L) T_r + L T_d$ , see Appendix C. Therefore,  $v < \frac{a' + b - \sqrt{(a' + b)^2 - 4a'b\epsilon}}{2a'b}$  results from Lemma 2, where  $\bar{\tau}$  is replaced by  $\bar{\tau}'$ .  $\square$

To illustrate the results of Corollary 1, we show  $\bar{\tau}'$  as a function of  $v$  in Fig. 4, where different codebook sizes and RIS response times are considered. As one can see, the overall overhead does not only increase with the codebook size, but also significantly depends on the RIS response time  $T_r$ . For example, for a fast RIS with  $T_r = 1 \mu\text{s}$ , Fig. 4 shows that the maximum overhead is below 10% if  $v < 20 \text{ km/h}$  and  $M_L \leq 512$ . In contrast, for a slow RIS with  $T_r = 1 \text{ ms}$ , the same low overhead is only achieved if  $v < 0.45 \text{ km/h}$ . However, we note that slow RISs with large  $T_r$  can still be efficiently configured using beam training if  $\bar{\tau} \ll \bar{\tau}'$ . For example, our numerical results in Section VI show that TS beam training achieves high effective rates for  $v > 20 \text{ km/h}$  and  $T_r = 1 \text{ ms}$ , see Fig. 8.

### B. Tradeoff Analysis

In the previous section, we have shown that for certain system parameters the performance may not be affected by the beam training overhead. In this section, we reveal how non-negligible overheads lead to different effective rates for FS, HS, and TS. Thereby, we assume  $M_1 > 8$ , which is a necessary condition for the considered TS beam training and may be required for providing sufficiently large reflection gains in practice [19]. For HS beam training, we assume  $\tilde{M} > 1$  and  $L > 1$ , and note that the codebook at level  $L$  is adopted for the single-level schemes, i.e., FS and TS beam training.

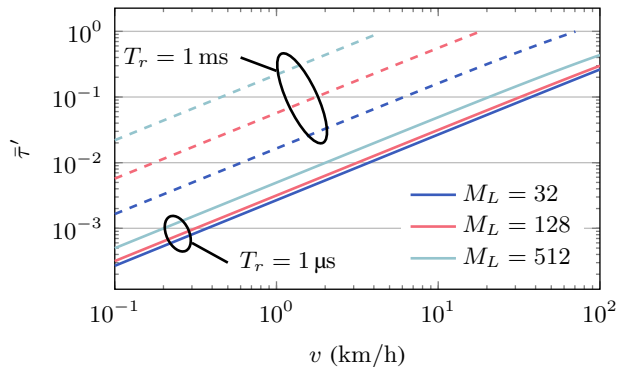


Fig. 4: Upper bound for overall overhead as a function of the user velocity, considering different codebook sizes and RIS response times  $T_r$  (cf. Table I); frame factor  $\nu = 0.15$ ,  $A = 100 \text{ m} \times 50 \text{ m}$ ,  $T_s = 1 \mu\text{s}$ ,  $T_d = 0.1 \text{ ms}$ , and  $N_{s,L} = 8$ .

*Lemma 3.* Assuming optimal codeword selection, TS beam training leads to higher effective rates than FS and HS beam training. Moreover, HS beam training outperforms FS beam training or vice versa, depending on the considered system parameters.

*Proof.* Due to optimal codeword selection and identical codebooks at the highest codebook level, all considered beam training strategies choose the same codeword and provide the same SNR for data transmission. Thus, one can see from (8) that FS, HS, and TS only result in different effective rates due to different overheads. Consequently, TS provides the highest effective rate because  $\bar{\tau}^{\text{TS}} < \bar{\tau}^{\text{FS}}$  and  $\bar{\tau}^{\text{TS}} < \bar{\tau}^{\text{HS}}$ , cf. (24)–(26). However,  $\bar{\tau}^{\text{FS}} > \bar{\tau}^{\text{HS}}$  or  $\bar{\tau}^{\text{FS}} < \bar{\tau}^{\text{HS}}$  may hold, depending on the system parameters in (24) and (25).  $\square$

Interestingly, Lemma 3 reveals that FS beam training outperforms HS beam training if  $\bar{\tau}^{\text{FS}} < \bar{\tau}^{\text{HS}}$ , which particularly happens, e.g., for fast RIS response times and large feedback delays. Further insight on this case is provided by the following lemma, where the above inequality is simplified to a lower bound on  $T_d$ .

*Lemma 4.* FS beam training provides a higher effective rate than HS beam training if

$$T_d > T_d^{\min} = \frac{M_L - \zeta}{L - 1} (T_r + T_s N_{s,L}). \quad (28)$$

*Proof.* Recall that the codebook for FS beam training is identical to that for HS beam training at level  $L$ . Thus, based on (1) and (2),  $\bar{\tau}^{\text{FS}} < \bar{\tau}^{\text{HS}}$  is equivalent to

$$T_d(L - 1) > T_r(M_L - \zeta) + T_s \left( N_{s,L} M_L - \sum_{l=1}^L N_{s,l} M_{t,l} \right). \quad (29)$$

Moreover, (9) and (14) imply  $N_{s,l} \geq N_{s,l+1}$ , which can be used to reformulate (29) as follows

$$T_d(L-1) > T_r(M_L - \zeta) + T_s \left( N_{s,L} M_L - N_{s,L} \sum_{l=1}^L M_{t,l} \right). \quad (30)$$

Finally, (30) is simplified to (28) by using  $\zeta = \sum_{l=1}^L M_{t,l}$ .  $\square$

It is worth noting that the above results are based on the assumption of reliable beam training, which cannot always be guaranteed in practice, cf. Remark 1. However, since reliable beam training is desired, practical systems are designed such that the number of erroneous codeword selections is small. Thus, it is expected that Lemmas 3 and 4 generally hold, which is verified by our numerical results in Section VI.

## VI. NUMERICAL RESULTS

In the previous sections, our analysis of the tradeoff between the achievable SNR and the beam training overhead was based on ideal illumination of the subareas and reliable codeword selection during beam training. In this section, these results are verified by numerical simulations, considering a Rician fading channel model, non-ideal phase-shift designs, and random user trajectories. For the following evaluation, we employ numerical simulations to compute the SNR for data transmission in (7) and the effective ergodic rate in (8), averaged over the channel realizations for a random user trajectory with a total length of 1000 m. As a benchmark and upper bound for the beam training performance, the RIS is configured with narrow beams that always focus on the known user location assuming zero training overhead.

The user trajectory follows the random direction mobility model [44], where the user travels along straight paths within the coverage area and randomly changes its direction at the boundary of the coverage area.

Instead of the idealized phase-shift design that perfectly reflects the power collected at the RIS to the targeted subareas, our numerical results are based on a practical phase-shift design to realize narrow and wide beams, respectively. More specifically, the codewords of the RIS beam codebook are realized by the quadratic phase-shift profile from [28], which is parameterized to illuminate a particular subarea of the coverage area. Although the achieved coverage can be improved with optimized phase-shift designs, we adopt the quadratic phase-shift design due to its analytical form and note that the performance gap to optimized designs is generally small [29], [40].

Furthermore, we consider a geometric Rician fading channel model, where the BS-RIS channel and the RIS-user channel are given by

$$\mathbf{H}_i = \sqrt{\text{PL}_i}(\bar{\mathbf{H}}_i + \tilde{\mathbf{H}}_i) \quad (31)$$

$$\mathbf{h}_r = \sqrt{\text{PL}_r}(\bar{\mathbf{h}}_r + \tilde{\mathbf{h}}_r), \quad (32)$$

respectively, and

$$\bar{\mathbf{H}}_i = \sqrt{K_i/(K_i + 1)}e^{j\varphi_i}\mathbf{a}_{\text{RIS}}(\theta_i, \phi_i)\mathbf{d}_{\text{BS}}^H(\omega) \quad (33)$$

$$\tilde{\mathbf{H}}_i = \sqrt{1/((K_i + 1)C_i)}\sum_{c=1}^{C_i}\tilde{h}_{i,c}\mathbf{a}_{\text{RIS}}(\theta_{i,c}, \phi_{i,c})\mathbf{d}_{\text{BS}}^H(\omega_c) \quad (34)$$

$$\bar{\mathbf{h}}_r = \sqrt{K_r/(K_r + 1)}e^{-j\varphi_r}\mathbf{d}_{\text{RIS}}(\theta_r, \phi_r) \quad (35)$$

$$\tilde{\mathbf{h}}_r = \sqrt{1/((K_r + 1)C_r)}\sum_{c=1}^{C_r}\tilde{h}_{r,c}\mathbf{d}_{\text{RIS}}(\theta_{r,c}, \phi_{r,c}). \quad (36)$$

In (31)–(36), for  $s \in \{i, r\}$ ,  $\text{PL}_s$ ,  $K_s$ ,  $\varphi_s$ , and  $C_s$  denote the path loss, Rician K-factor, phase of the LoS path, and number of non-line-of-sight (NLoS) paths, respectively, and  $\omega$  denotes the AoD at the BS. Moreover, the AoAs and AoDs of the NLoS paths are indexed by  $c \in \{1, \dots, C_s\}$ , and the path coefficient of the  $c$ th NLoS path is given by  $\tilde{h}_{s,c} \sim \mathcal{CN}(0, 1)$ . The  $(q_x, q_y)$ th element of  $\mathbf{a}_{\text{RIS}}(\theta_i, \phi_i)$  and  $\mathbf{d}_{\text{RIS}}(\theta_r, \phi_r)$  as well as the  $n$ th element of  $\mathbf{d}_{\text{BS}}(\omega)$  are given by  $e^{j\frac{2\pi}{\lambda}(d_x q_x \sin(\theta_i) \cos(\phi_i) + d_y q_y \sin(\theta_i) \sin(\phi_i))}$ ,  $e^{-j\frac{2\pi}{\lambda}(d_x q_x \sin(\theta_r) \cos(\phi_r) + d_y q_y \sin(\theta_r) \sin(\phi_r))}$  and  $e^{-j\frac{2\pi}{\lambda}dn \sin(\omega)}$ , respectively, where  $q_x, q_y \in \{0, \dots, \sqrt{Q} - 1\}$  denote two-dimensional indices of the RIS unit cells and  $n \in \{0, \dots, N_{\text{BS}} - 1\}$ .

### A. System Parameters

Our theoretical analysis has shown that the performance tradeoff between overhead and achievable SNR depends on several different system parameters, including the codebook size, coverage area size, RIS size, transmit power, and number of pilot symbols. Therefore, in the following, we focus on typical RIS deployments and realistic timing constraints in order to evaluate practical scenarios. We consider user velocities  $v \in [3 \text{ km/h}, 100 \text{ km/h}]$  and RIS response times  $T_r \in [100 \text{ ns}, 1 \text{ ms}]$  in order to capture different mobility scenarios and RIS technologies. Unless otherwise noted, the feedback delay is set to  $T_d = 0.1 \text{ ms}$ , which is targeted by 3GPP for future systems [17], [45].

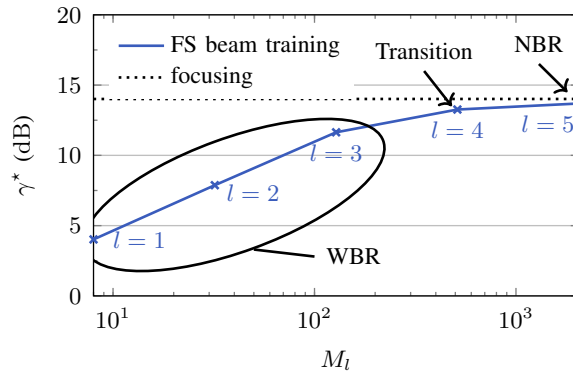


Fig. 5: SNR in (7) as a function of codebook size for  $N_{s,l} = 8$  and  $v = 3$  km/h. The corresponding levels of a hierarchical codebook are indicated by cross markers.

We adopt codebook sizes up to  $M_l = 2048$ , which corresponds to a hierarchical codebook with up to  $L = 5$  levels assuming  $M_1 = 8$  and  $\tilde{M} = 4$ . When comparing the performances of the considered beam training strategies, FS and TS beam training use the same codewords as specified by the highest codebook level for HS beam training.

Moreover, the RIS, the BS, and the center of the coverage area are located at coordinates  $(0 \text{ m}, 0 \text{ m}, 0 \text{ m})$ ,  $(0 \text{ m}, 40 \text{ m}, 50 \text{ m})$ , and  $(-10 \text{ m}, -20 \text{ m}, 100 \text{ m})$ , respectively. The coverage area has dimensions  $A_y = 100 \text{ m}$  and  $A_z = 50 \text{ m}$  and is partitioned into subareas of equal size, resulting in  $\mu = \sqrt{(A_y M_{L,x})^2 + (A_z M_{L,y})^2}$ . The RIS unit cell and BS antenna spacing are given by  $d = d_x = d_y = \lambda/2$ . The BS has  $N_{\text{BS}} = 16$  antenna elements and steers its main lobe towards the center of the RIS. For the channels, we assume  $C_i = C_r = 6$  and  $K_i = K_r = 4$ , and  $\text{PL}_i$  and  $\text{PL}_r$  are given by the free-space path loss model. The azimuth angles  $(\phi_{i,c}, \phi_{r,c})$  and elevation angles  $(\theta_{i,c}, \theta_{r,c})$  of the NLoS paths are drawn from uniform distributions  $\mathcal{U}(0, 2\pi)$  and  $\mathcal{U}(0, \pi/2)$ , respectively. Furthermore, we assume antenna element gains  $G_{\text{TX}} = G_{\text{RX}} = 1$ , transmit power  $P = 15 \text{ dBm}$ , channel estimation overhead  $\tau_e = 40T_s$  [46], frame factor  $\nu = 0.15$ , carrier frequency  $28 \text{ GHz}$ , signal bandwidth  $B = 1/T_s = 1 \text{ MHz}$ , and  $\sigma^2 = N_0 F B$  with noise power spectral density  $N_0 = -174 \text{ dBm/Hz}$  and noise figure  $F = 6 \text{ dB}$ . Additional parameters are individually given for each figure.

### B. SNR Regimes

We first evaluate the impact of the codebook size on the achievable SNR by comparing the numerical results for beam training and with that for focusing. In Fig. 5, we show the results for

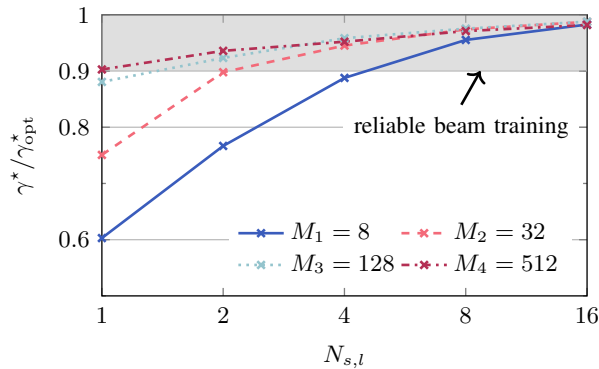


Fig. 6: Beam training reliability as a function of the number of pilot symbols for  $v = 3$  km/h and different codebook sizes corresponding to  $L = 4$  codebook levels.

FS beam training as a function of the codebook size, and indicate the corresponding codebook levels of a hierarchical codebook by cross markers. One can see that  $\gamma^*$  increases with  $M_l$  if the codebook is small but saturates at the upper bound for large  $M_l$ . The reason is that, for a given coverage area, the size of the subareas is inversely proportional to the codebook size, leading to a change of SNR regime as  $M_l$  grows. For example, note that the SNR achieved by beam training is similar to that for focusing if  $M_l > 500$ . In this case, the subareas are sufficiently small to be approximately illuminated by narrow beams. However, a lower SNR is observed for  $M_l < 500$  because wide beams are required to distribute the power collected by the RIS to larger subareas. These results accurately match the scaling laws in Proposition 1, which states that the SNR linearly scales with  $M_l$  in the WBR and is independent of  $M_l$  in the NBR. Moreover, the markers Fig. 5 show that the system operates in different SNR regimes during HS beam training with  $L = 5$  levels. In particular, the SNR is in the WBR, the transition regime, and the NBR for  $l \leq 3$ ,  $l = 4$ , and  $l = 5$ , respectively, which confirms the analytical results shown in Fig. 3.

### C. Overhead Regimes

In order to evaluate the impact of the number of pilot symbols on the SNR achieved by beam training, we adopt the ratio  $\gamma^*/\gamma_{\text{opt}}^*$  as a measure for the beam training reliability, where  $\gamma_{\text{opt}}^*$  denotes the SNR for data transmission achieved by optimal codeword selection. Thus,  $\gamma_{\text{opt}}^*$  represents the SNR that can be achieved without the impact of channel fading or receiver noise. Moreover, we assume that beam training can be considered reliable if  $\gamma^*/\gamma_{\text{opt}}^* > 0.9$ . For the considered system parameters, Fig. 6 shows that reliable beam training is only achieved when

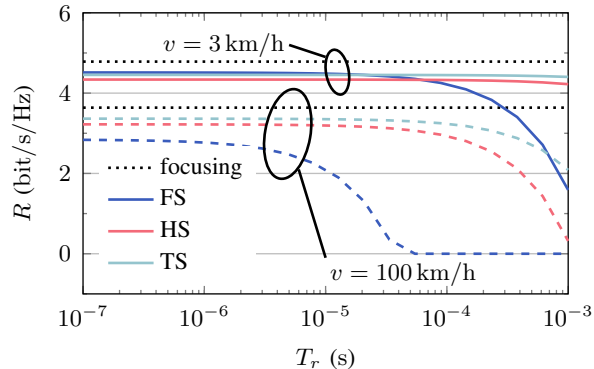


Fig. 7: Effective rate as a function of the RIS response time for  $N_{s,l} = 8$ ,  $L = 4$ ,  $v = 3$  km/h (solid lines), and  $v = 100$  km/h (dashed lines).

$N_{s,l}$  or  $M_l$  is large. Otherwise, the beam training reliability is significantly reduced, which can be explained by a larger number of erroneous codeword selections owing to a low SNR. These observations are consistent with (14) and the definitions of SPR and MPR in Section III-B. For example, the numerical results in Fig. 6 reveal that SPR holds for  $M_l = 512$  because  $\gamma^*/\gamma_{\text{opt}}^* > 0.9$  is achieved with  $N_{s,l} = 1$ . In contrast, MPR holds for  $M_l \leq 128$  where  $N_{s,l} > 1$  is required to obtain  $\gamma^*/\gamma_{\text{opt}}^* > 0.9$ .

#### D. Impact of RIS Response Time and User Velocity

Since our theoretical analysis has shown that both the RIS response time and the user velocity can have a significant impact on the system performance, we evaluate the effective rate for different values of  $T_r$  and  $v$  in Fig. 7. For  $v = 3$  km/h, one can see that all considered beam training strategies provide a similar effective rate as focusing if  $T_r < 100$   $\mu\text{s}$ , and only FS beam training results in reduced rates if  $T_r > 100$   $\mu\text{s}$ . In contrast, one observes significant performance differences for  $v = 100$  km/h. These results suggest that, for a slowly moving user, the beam training overhead is negligible if the RIS response time is less than 100  $\mu\text{s}$ , which can be realized with RISs based on PIN diodes or MEMS, cf. Table I. In this case, FS is the preferred beam training strategy because decision and tracking errors may reduce the SNR achieved by HS and TS beam training, respectively. Although not significant, this effect can be seen in Fig. 7 for  $T_r < 10$   $\mu\text{s}$  and  $v = 3$  km/h, where the effective rates for HS and TS beam training are slightly lower than that for FS beam training. However, FS beam training provides the worst performance if  $v = 100$  km/h. In this case, Fig. 7 demonstrates that low-overhead beam training is essential

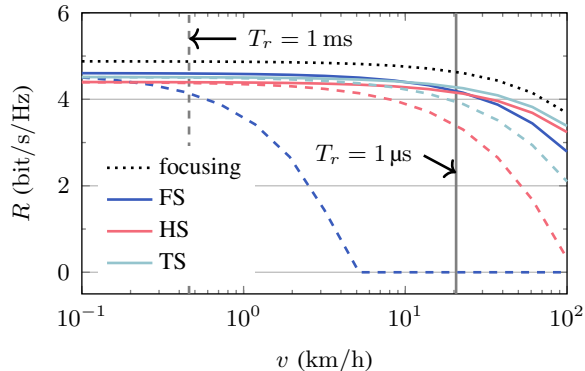


Fig. 8: Effective rate as a function of the user velocity for  $L = 4$ ,  $T_r = 1 \mu\text{s}$  (solid lines), and  $T_r = 1 \text{ms}$  (dashed lines). The values of the bound  $v^{\max}$  in (27) for  $\epsilon = 0.1$  are indicated by the vertical lines.

for achieving high effective rates, especially for RIS technologies with a slow response time in the order of milliseconds, e.g., based on liquid crystal.

More insight on the impact of the overhead on the system performance is provided in Fig. 8, which shows the effective rate as a function of the user velocity for  $T_r \in \{1 \mu\text{s}, 1 \text{ms}\}$ . One can see that a fast RIS with  $T_r = 1 \mu\text{s}$  (solid lines in Fig. 8) enables beam training for high user velocities without significant performance loss, in particular, if HS or TS beam training is applied. In contrast, employing a slow RIS with  $T_r = 1 \text{ms}$  reduces the performance for all considered beam training strategies. The most significant impact is observed for FS beam training, where the largest velocity that has negligible impact on  $R$  decreases from about 20 km/h to 0.4 km/h. As indicated by the vertical lines in Fig. 8, these results accurately match the analytical bound  $v^{\max}$  in (27) for  $\epsilon = 0.1$ .

### E. Impact of Feedback Delay

Finally, we evaluate the effective rate as a function of the feedback delay in Fig. 9, considering a fast RIS with response times  $T_r = 1 \mu\text{s}$  (solid lines) and  $T_r = 30 \mu\text{s}$  (dashed lines). The results show that the effective rates are approximately constant for  $T_d < 1 \text{ms}$ , but decrease for larger values of  $T_d$ . Moreover, one can see that TS provides the best beam training performance, whereas HS beam training outperforms FS beam training or vice versa, depending on the values of  $T_d$  and  $T_r$ . This is consistent with our theoretical results of Lemma 3 and can be explained by the fact that HS beam training involves multiple feedback transmissions, which cause a large overhead if  $T_d$  is large. Thus, if the RIS response time is relatively short, FS beam training can

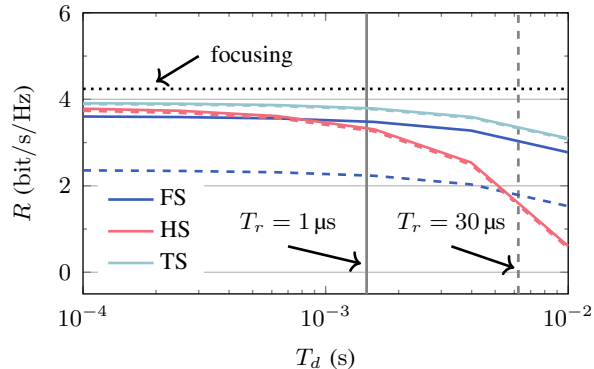


Fig. 9: Effective rate as a function of the feedback delay for  $L = 4$ ,  $v = 50$  km/h,  $T_r = 1 \mu\text{s}$  (solid lines), and  $T_r = 30 \mu\text{s}$  (dashed lines). The values of the bound  $T_d^{\min}$  in (28) are indicated by the vertical lines.

have a lower overhead than HS beam training, leading to a larger effective rate. In Fig. 9, this happens for  $T_d > 0.9$  ms ( $T_r = 1 \mu\text{s}$ ) and  $T_d > 6$  ms ( $T_r = 30 \mu\text{s}$ ). As indicated by the vertical lines, these results are accurately captured by the lower bound  $T_d^{\min}$  in (28).

## VII. CONCLUSION

This paper studied the performance tradeoff between the overhead and achievable SNR in RIS beam training, considering the size of the coverage, the RIS response time, and the feedback delay. In particular, we derived scaling laws for the achievable SNR based on narrow and wide beam designs, and showed that the overhead for reliable beam training is either dependent on or independent of the SNR. Based on these insights, we investigated the impact of the overhead for FS, HS, and TS beam training on the effective rate, and provided an upper bound on the user velocity for which the overhead is negligible. Moreover, when the overhead is not negligible, we showed that TS beam training achieves higher effective rates than HS and FS beam training, while we revealed that HS beam training may or may not outperform FS beam training. Furthermore, our theoretical results were verified by numerical simulations. In particular, our numerical results demonstrated that fast RISs facilitate FS beam training, whereas large feedback delays can significantly reduce the performance for HS beam training.

## APPENDIX

## A. SNR Scaling Laws

In this section, we derive the scaling laws of the achievable SNR for wide beams and narrow beams, respectively.

1) *Wide-Beam Design*: Assuming free-space propagation and a precoding vector  $\mathbf{f}$  that aligns the main lobe of the BS with the LoS path to the RIS, a signal transmitted at the BS causes power density  $S_i = \frac{PG_{\text{TX}}N_{\text{BS}}}{4\pi d_i^2}$  at the RIS, where  $d_i$  denotes the distance between the BS and the RIS. Moreover, the effective area of the RIS is given by  $A_{\text{RIS}} = d_x d_y Q \tilde{a}_{\text{RIS}}$ , where  $\tilde{a}_{\text{RIS}}$  accounts for the AoA and polarization of the incident wave [8], [12]. Thus, the power collected by the RIS is given by  $P_i = S_i d_x d_y Q \tilde{a}_{\text{RIS}}$  [1]. Furthermore, for the idealized wide-beam design and subareas of equal size, the  $m$ th codeword at the  $l$ th codebook level perfectly distributes the collected power  $P_i$  across an area of size  $A/M_l$ , where  $A/M_l$  is larger than  $r_m^{\min}$ , i.e., the beam footprint that results from focusing on one single direction. Then, the power density at a location within the subarea is given by  $S_{r,l} = P_i \frac{M_l}{A}$  [1], which leads to achievable SNR

$$\bar{\gamma}_{m,l} = \frac{S_{r,l} A_{\text{RX}}}{\sigma^2} = \frac{PG_{\text{TX}}N_{\text{BS}}G_{\text{RX}}}{\sigma^2} \frac{\lambda^2 d_x d_y \tilde{a}_{\text{RIS}}}{(4\pi d_i)^2 A} Q M_l, \quad (37)$$

where  $A_{\text{RX}} = \lambda^2 G_{\text{RX}} / (4\pi)$  denotes the effective receive antenna area.

2) *Narrow-Beam Design*: A codebook with narrow beams corresponds to sampling the coverage area in the angular space, where the  $m$ th codeword at the  $l$ th codebook level results in a narrow beam focusing on a particular direction  $(\theta_{m,l}, \phi_{m,l})$ . Here, we assume that  $(\theta_{m,l}, \phi_{m,l})$  denotes the direction to the center of the  $m$ th subarea for the  $l$ th codebook level. Then, the achievable SNR is given by [8]

$$\bar{\gamma}_{m,l} = \frac{PG_{\text{TX}}N_{\text{BS}}G_{\text{RX}}}{\sigma^2} \frac{\lambda^2 \lambda^2 |g(\theta_{m,l}, \phi_{m,l})|^2}{(4\pi d_i)^2 (4\pi d_r)^2}, \quad (38)$$

where  $d_r$  and  $|g(\theta_{m,l}, \phi_{m,l})|^2$  denote the RIS-user distance and the RIS gain for the  $m$ th codeword at the  $l$ th codebook level, respectively. For a user located in direction  $(\theta_r, \phi_r)$ , the RIS gain is given by [8]

$$|g(\theta_{m,l}, \phi_{m,l})|^2 = |g_{\text{UC}}|^2 \left| \frac{\sin(\sqrt{Q}W_x)}{\sin(W_x)} \frac{\sin(\sqrt{Q}W_y)}{\sin(W_y)} \right|^2, \quad (39)$$

where  $W_o = \frac{\pi d_o}{\lambda} (w_o(\theta_r, \phi_r) - w_o(\theta_{m,l}, \phi_{m,l}))$ ,  $o \in \{x, y\}$ , for  $w_x(\theta, \phi) = \sin(\theta) \cos(\phi)$  and  $w_y(\theta, \phi) = \sin(\theta) \sin(\phi)$ . Moreover, if the subareas of the coverage area are significantly smaller

than the footprint of a narrow beam, one can always find a codeword that approximately provides the maximum RIS gain for any direction  $(\theta_r, \phi_r)$ . Since  $|g(\theta_{m,l}, \phi_{m,l})|^2 \leq |g_{\text{UC}}|^2 Q^2$  [8], the SNR in (38) can be written as

$$\bar{\gamma}_{m,l} \approx \frac{PG_{\text{TX}}N_{\text{BS}}G_{\text{RX}}}{\sigma^2} \frac{\lambda^2 \lambda^2 |g_{\text{UC}}|^2 Q^2}{(4\pi d_i)^2 (4\pi d_r)^2}. \quad (40)$$

### B. Proof of Lemma 2

We need to show that a user velocity  $v > \frac{a+b+\sqrt{(a+b)^2-4abe}}{2ab}$  results in zero time for data transmission. For the considered transmission protocol, cf. Fig. 2, this case is true for  $T_f \leq \tau_t + \tau_e$ , which is equivalent to  $\frac{1}{a(1+\tau_e/\tau_t)} \leq v$ . Thus, the proof is completed if we show that  $\frac{1}{a(1+\tau_e/\tau_t)} \leq \frac{a+b+\sqrt{(a+b)^2-4abe}}{2ab}$  holds. Since  $\tau_t \geq 0$ ,  $\tau_e \geq 0$ , and  $\epsilon < 1$ , the above condition is certainly true if  $a - b + \sqrt{(a+b)^2 - 4ab} \geq 0$ . For  $a > 0$  and  $b > 0$ , this can be rewritten as  $a - b + |a - b| \geq 0$ , which is true.

### C. Proof of Corollary 1

In order to find an upper bound  $\tau_t^{\max} \geq \max_{x \in \{\text{FS}, \text{HS}, \text{TS}\}} \tau_t^x$ , we note that MPR and WBR cause the largest overhead because they require a larger number of pilot symbols compared to SPR and NBR. Moreover, a comparison of (16) and (20) shows that the overhead for FS beam training is always larger than that for TS beam training if  $M_l > 8$  is assumed. Thus, it is sufficient to compare the overheads for FS beam training and HS beam training.

The considered HS beam training is based on a codebook that grows by a factor of  $\tilde{M}$  with each level. Thus, in the WBR, the SNR increases by  $\tilde{M}$  at each codebook level, which implies that the number of required pilot symbols decreases as  $N_{s,l+1} = N_{s,l}/\tilde{M}$ . Rewriting the latter as  $N_{s,l} = \tilde{M}^{L-l} N_{s,L}$  leads to an upper bound for  $\tau_t^{\text{HS}}$  as follows

$$\tau_t^{\text{HS}} = T_r (1 + \zeta) + T_d L + T_s \sum_{l=1}^L N_{s,l} M_{t,l} \quad (41a)$$

$$\stackrel{(a)}{=} T_r (1 + \zeta) + T_d L + T_s N_{s,L} \left( M_L + \frac{\tilde{M}^{L-1} - 1}{1 - 1/\tilde{M}} \right) \quad (41b)$$

$$\stackrel{(b)}{<} T_r (1 + \zeta) + T_d L + T_s N_{s,L} M_L 1.25, \quad (41c)$$

where (a) is based on the partial sum of a geometric series and (b) results from  $\tilde{M} \geq 2$  and  $M_1 > 8$ . Then, combining (41c) and  $\tau_t^{\text{FS}} = T_s N_{s,L} M_L + T_r (1 + M_L) + T_d$  yields

$$\tau_t^{\max} = 1.25 N_{s,L} M_L T_s + (1 + M_L) T_r + L T_d. \quad (42)$$

## REFERENCES

- [1] F. Laue, M. Garkisch, V. Jamali, and R. Schober, "Performance tradeoff of RIS beam training: Overhead vs. achievable SNR," in *Proc. IEEE 56th Asilomar Conf. Signals, Systems, and Comput.*, Oct. 2022.
- [2] M. D. Renzo, A. Zappone, M. Debbah, M.-S. Alouini, C. Yuen, J. de Rosny, and S. Tretyakov, "Smart radio environments empowered by reconfigurable intelligent surfaces: How it works, state of research, and the road ahead," *IEEE J. Sel. Areas Commun.*, vol. 38, no. 11, pp. 2450–2525, Jul. 2020.
- [3] S. Gong, X. Lu, D. T. Hoang, D. Niyato, L. Shu, D. I. Kim, and Y.-C. Liang, "Toward smart wireless communications via intelligent reflecting surfaces: A contemporary survey," *IEEE Commun. Surveys & Tut.*, vol. 22, no. 4, pp. 2283–2314, fourthquarter 2020.
- [4] Q. Wu, S. Zhang, B. Zheng, C. You, and R. Zhang, "Intelligent reflecting surface-aided wireless communications: A tutorial," *IEEE Trans. Commun.*, vol. 69, no. 5, pp. 3313–3351, May 2021.
- [5] C. Pan, G. Zhou, K. Zhi, S. Hong, T. Wu, Y. Pan, H. Ren, M. D. Renzo, A. L. Swindlehurst, R. Zhang, and A. Y. Zhang, "An overview of signal processing techniques for RIS/IRS-aided wireless systems," *IEEE J. Sel. Topics Signal Process.*, vol. 16, no. 5, pp. 883–917, Aug. 2022.
- [6] B. Zheng, C. You, W. Mei, and R. Zhang, "A survey on channel estimation and practical passive beamforming design for intelligent reflecting surface aided wireless communications," *IEEE Commun. Surveys & Tut.*, vol. 24, no. 2, pp. 1035–1071, secondquarter 2022.
- [7] J. An, C. Xu, Q. Wu, D. W. K. Ng, M. D. Renzo, C. Yuen, and L. Hanzo, "Codebook-based solutions for reconfigurable intelligent surfaces and their open challenges," *IEEE Wirel. Commun.*, Nov. 2022.
- [8] M. Najafi, V. Jamali, R. Schober, and H. V. Poor, "Physics-based modeling and scalable optimization of large intelligent reflecting surfaces," *IEEE Trans. Commun.*, vol. 69, no. 4, pp. 2673–2691, Dec. 2020.
- [9] R. Liu, J. Dou, P. Li, J. Wu, and Y. Cui, "Simulation and field trial results of reconfigurable intelligent surfaces in 5G networks," *IEEE Access*, vol. 10, pp. 122 786–122 795, 2022.
- [10] Z. Peng, G. Zhou, C. Pan, H. Ren, A. L. Swindlehurst, P. Popovski, and G. Wu, "Channel estimation for RIS-aided multi-user mmWave systems with uniform planar arrays," *IEEE Trans. Commun.*, vol. 70, no. 12, pp. 8105–8122, Dec. 2022.
- [11] J. Wang, W. Tang, S. Jin, C.-K. Wen, X. Li, and X. Hou, "Hierarchical codebook-based beam training for RIS-assisted mmWave communication systems," *IEEE Trans. Commun.*, vol. 71, no. 6, pp. 3650–3662, Jun. 2023.
- [12] V. Jamali, G. C. Alexandropoulos, R. Schober, and H. V. Poor, "Low-to-zero-overhead IRS reconfiguration: Decoupling illumination and channel estimation," *IEEE Commun. Lett.*, vol. 26, no. 4, pp. 932–936, Apr. 2022.
- [13] Y. Zhang, B. Di, H. Zhang, M. Dong, L. Yang, and L. Song, "Dual codebook design for intelligent omni-surface aided communications," *IEEE Trans. Wireless Commun.*, vol. 21, no. 11, pp. 9232–9245, Nov. 2022.
- [14] S. Zhang, Y. Zhang, H. Zhang, N. Ye, and B. Di, "Rate-overhead tradeoff for IOS-aided beam training: How large codebook is enough for the IOS?" *IEEE Wireless Commun. Lett.*, vol. 12, no. 6, pp. 1081–1085, Jun. 2023.
- [15] S. Zhang, Y. Zhang, B. Di, and H. Zhang, "Rate-overhead tradeoff in beam training for RRS-assisted multi-user communications," in *Proc. IEEE 96th Veh. Technol. Conf.*, Sep. 2022.
- [16] F. Hamidi-Sephehr, M. Sajadieh, S. Panteleev, T. Islam, I. Karls, D. Chatterjee, and J. Ansari, "5G URLLC: Evolution of high-performance wireless networking for industrial automation," *IEEE Commun. Standards Mag.*, vol. 5, no. 2, pp. 132–140, Jun. 2021.
- [17] B. Ji, Y. Han, S. Liu, F. Tao, G. Zhang, Z. Fu, and C. Li, "Several key technologies for 6G: Challenges and opportunities," *IEEE Commun. Standards Mag.*, vol. 5, no. 2, pp. 44–51, Jun. 2021.

- [18] A. Jiménez-Sáez, A. Asadi, R. Neuder, M. Delbari, and V. Jamali, "Reconfigurable intelligent surfaces with liquid crystal technology: A hardware design and communication perspective," Aug. 2023. [Online]. Available: <https://arxiv.org/abs/2308.03065>
- [19] P. Wang, J. Fang, W. Zhang, Z. Chen, H. Li, and W. Zhang, "Beam training and alignment for RIS-assisted millimeter-wave systems: State of the art and beyond," *IEEE Wirel. Commun.*, vol. 29, no. 6, pp. 64–71, Dec. 2022.
- [20] H. Kamoda, T. Iwasaki, J. Tsumochi, T. Kuki, and O. Hashimoto, "60-GHz electronically reconfigurable large reflectarray using single-bit phase shifters," *IEEE Trans. Antennas Propag.*, vol. 59, no. 7, pp. 2524–2531, Jul. 2011.
- [21] H. Yang, F. Yang, S. Xu, Y. Mao, M. Li, X. Cao, and J. Gao, "A 1-bit 10x10 reconfigurable reflectarray antenna: Design, optimization, and experiment," *IEEE Trans. Antennas Propag.*, vol. 64, no. 6, pp. 2246–2254, Jun. 2016.
- [22] Y. Li, J. Eisenbeis, X. Wan, S. Bettinga, X. Long, M. B. Alabd, J. Kowalewski, T. Cui, and T. Zwick, "A programmable-metasurface-based TDMA fast beam switching communication system at 28 GHz," *IEEE Antennas Wirel. Propag. Lett.*, vol. 20, no. 5, pp. 658–662, May 2021.
- [23] X. Pan, F. Yang, S. Xu, and M. Li, "A 10 240-element reconfigurable reflectarray with fast steerable monopulse patterns," *IEEE Trans. Antennas Propag.*, vol. 69, no. 1, pp. 173–181, Jan. 2021.
- [24] N. Sharma, R. Smitha, D. Kumar, and A. S. Siddiqui, "Design, simulation and a comparative study of square, rectangular, triangular and dual beamed RF MEMS switch for switching applications," in *Proc. IEEE 4th Int. Conf. Signal Process. Integr. Netw.*, Feb. 2017.
- [25] K. G. Sravani, D. Prathyusha, K. S. Rao, P. A. Kumar, G. S. Lakshmi, C. G. Chand, P. Naveena, L. N. Thalluri, and K. Guha, "Design and performance analysis of low pull-in voltage of dimple type capacitive RF MEMS shunt switch for ka-band," *IEEE Access*, vol. 7, pp. 44 471–44 488, 2019.
- [26] A. Nooraiyeen, G. Priya, N. K. Kavya, V. Sanchitha, and S. B. Rudraswamy, "Design of novel low actuation voltage shunt capacitive RF MEMS switch," in *Proc. IEEE Int. Conf. Smart Electron. Commun.*, Sep. 2020.
- [27] R. Jakoby, A. Gaebler, and C. Weickhmann, "Microwave liquid crystal enabling technology for electronically steerable antennas in SATCOM and 5G millimeter-wave systems," *Crystals*, vol. 10, no. 6, p. 514, Jun. 2020.
- [28] V. Jamali, M. Najafi, R. Schober, and H. V. Poor, "Power efficiency, overhead, and complexity tradeoff of IRS codebook design - quadratic phase-shift profile," *IEEE Commun. Lett.*, vol. 25, no. 6, pp. 2048–2052, Jun. 2021.
- [29] W. R. Ghanem, V. Jamali, M. Schellmann, H. Cao, J. Eichinger, and R. Schober, "Optimization-based phase-shift codebook design for large IRSs," *IEEE Commun. Lett.*, vol. 27, no. 2, pp. 635–639, Feb. 2023.
- [30] S. Lv, Y. Liu, X. Xu, A. Nallanathan, and A. L. Swindlehurst, "RIS-aided near-field MIMO communications: Codebook and beam training design," Sep. 2023. [Online]. Available: <https://arxiv.org/abs/2310.00294>
- [31] C. You, B. Zheng, and R. Zhang, "Fast beam training for IRS-assisted multiuser communications," *IEEE Wireless Commun. Lett.*, vol. 9, no. 11, pp. 1845–1849, Nov. 2020.
- [32] G. C. Alexandropoulos, V. Jamali, R. Schober, and H. V. Poor, "Near-field hierarchical beam management for RIS-enabled millimeter wave multi-antenna systems," in *Proc. IEEE 12th Sensor Array and Multichannel Signal Process. Workshop*, Jun. 2022.
- [33] W. Liu, C. Pan, H. Ren, F. Shu, S. Jin, and J. Wang, "Low-overhead beam training scheme for extremely large-scale RIS in near field," *IEEE Trans. Commun.*, vol. 71, no. 8, pp. 4924–4940, Aug. 2023.
- [34] X. Wang, Z. Lin, F. Lin, and L. Hanzo, "Joint hybrid 3D beamforming relying on sensor-based training for reconfigurable intelligent surface aided TeraHertz-based multiuser massive MIMO systems," *IEEE Sensors J.*, vol. 22, no. 14, pp. 14 540–14 552, Jul. 2022.
- [35] H. Huang, C. Zhang, Y. Zhang, B. Ning, H. Gao, S. Fu, K. Qiu, and Z. Han, "Two-timescale-based beam training for

- RIS-aided millimeter-wave multi-user MISO systems,” *IEEE Trans. Veh. Technol.*, vol. 72, no. 9, pp. 11 884–11 897, Sep. 2023.
- [36] W. Wang and W. Zhang, “Joint beam training and positioning for intelligent reflecting surfaces assisted millimeter wave communications,” *IEEE Trans. Wireless Commun.*, vol. 20, no. 10, pp. 6282–6297, Oct. 2021.
- [37] X. Tian and Z. Sun, “Fast beam tracking for reconfigurable intelligent surface assisted mobile mmWave networks,” Feb. 2021. [Online]. Available: <https://arxiv.org/abs/2102.11414>
- [38] A. M. Romanov, F. Gringoli, and A. Sikora, “A precise synchronization method for future wireless TSN networks,” *IEEE Trans. Ind. Inf.*, vol. 17, no. 5, pp. 3682–3692, May 2021.
- [39] T. S. Rappaport, *Wireless Communications*. Prentice Hall PTR, 2001.
- [40] F. Laue, V. Jamali, and R. Schober, “IRS-assisted active device detection,” in *Proc. IEEE 22nd Int. Workshop Signal Process. Advances in Wireless Commun.*, Sep. 2021.
- [41] H. Han, Y. Liu, and L. Zhang, “On half-power beamwidth of intelligent reflecting surface,” *IEEE Commun. Lett.*, vol. 25, no. 4, pp. 1333–1337, Apr. 2021.
- [42] X. Wei, L. Dai, Y. Zhao, G. Yu, and X. Duan, “Codebook design and beam training for extremely large-scale RIS: Far-field or near-field?” *China Commun.*, vol. 19, no. 6, pp. 193–204, Jun. 2022.
- [43] L. Yang and W. Zhang, “Hierarchical codebook and beam alignment for UAV communications,” in *Proc. IEEE Globecom Workshops*, Dec. 2018.
- [44] T. Camp, J. Boleng, and V. Davies, “A survey of mobility models for ad hoc network research,” *Wireless Commun. Mob. Comput.*, vol. 2, no. 5, pp. 483–502, Sep. 2002.
- [45] B. Hassan, S. Baig, and M. Asif, “Key technologies for ultra-reliable and low-latency communication in 6G,” *IEEE Commun. Standards Mag.*, vol. 5, no. 2, pp. 106–113, Jun. 2021.
- [46] P. Wang, J. Fang, H. Duan, and H. Li, “Compressed channel estimation for intelligent reflecting surface-assisted millimeter wave systems,” *IEEE Signal Process Lett.*, vol. 27, pp. 905–909, May 2020.